Hindawi Publishing Corporation
Discrete Dynamics in Nature and Society
Volume 2011, Article ID 862494, 27 pages
doi:10.1155/2011/862494

Research Article

Codimension-Two Bifurcations of Fixed Points in a Class of Discrete Prey-Predator Systems

R. Khoshsiar Ghaziani,[1] W. Govaerts,[2] and C. Sonck[2]

[1] *Department of Applied Mathematics and Computer Science, Shahrekord University, P.O. Box 115, Saman Road, Shahrekord 88186-34141, Iran*
[2] *Department of Applied Mathematics and Computer Science, Ghent University, Krijgslaan 281-S9, 9000 Gent, Belgium*

Correspondence should be addressed to R. Khoshsiar Ghaziani, khoshsiar@sci.sku.ac.ir

Received 9 December 2010; Revised 7 March 2011; Accepted 20 March 2011

Academic Editor: Juan J. Nieto

The dynamic behaviour of a Lotka-Volterra system, described by a planar map, is analytically and numerically investigated. We derive analytical conditions for stability and bifurcation of the fixed points of the system and compute analytically the normal form coefficients for the codimension 1 bifurcation points (flip and Neimark-Sacker), and so establish sub- or supercriticality of these bifurcation points. Furthermore, by using numerical continuation methods, we compute bifurcation curves of fixed points and cycles with periods up to 16 under variation of one and two parameters, and compute all codimension 1 and codimension 2 bifurcations on the corresponding curves. For the bifurcation points, we compute the corresponding normal form coefficients. These quantities enable us to compute curves of codimension 1 bifurcations that branch off from the detected codimension 2 bifurcation points. These curves form stability boundaries of various types of cycles which emerge around codimension 1 and 2 bifurcation points. Numerical simulations confirm our results and reveal further complex dynamical behaviours.

1. Introduction

The dynamic relationship between predators and their prey is one of the dominant themes in both ecology and mathematical ecology due to its universal existence and importance; see [1–6]. The prototype Lotka-Volterra predator-prey system has received a lot of attention from theoretical and mathematical biologists; see [2–6]. This model is described by the following system of ordinary differential equations:

$$\begin{aligned} \dot{x}(t) &= x(r_1 - a_{11}x) - a_{12}xy, \\ \dot{y}(t) &= y(-r_2 - a_{22}y) + a_{21}xy, \end{aligned} \tag{1.1}$$

where $x(t)$ and $y(t)$ represent the densities of the prey and the predator, r_1, a_{12}, r_2, and a_{21} are the intrinsic growth rate of the prey, the capture rate, the death rate of the predator, and the conversion rate, respectively, a_{11} and a_{22} denote the intraspecific competition coefficients of the prey and the predator, and r_1/a_{11} is the carrying capacity of the prey.

This and related models have been studied intensively in the previous decades and it has been noted, in particular, that they present a wealth of bifurcations of various codimensions. Organizing centers of codimension 3 have been investigated in great detail in [7] and references therein. For background on bifurcation theory, we refer to [8, 9].

Far-reaching generalizations of the model have been studied both analytically and numerically. We refer in particular to [10] where a five-parameter family of planar vector fields is studied that takes into account group defense strategy, competition between predators and a nonmonotonic response function. Though mathematical analysis is the prime tool also in this case, numerical methods are indispensable for a detailed study. In [10] not only the general-purpose languages Mathematica and Matlab were used, but also the dedicated bifurcation packages AUTO [11] and MatCont [12].

However, in recent years, many authors [4–6, 13] have suggested that discrete-time models are more appropriate than continuous ones, especially when the populations have nonoverlapping generations. Furthermore, discrete-time models often provide very effective approximations to continuous models which cannot be solved explicitly.

Though discrete models are by no means less complex than continuous ones, they have the computational (numerical) advantage that no differential equations have to be solved. In fact, the state-of-the-art in computational bifurcation study is in some respects more advanced for discrete systems than for continuous ones. So far, normal form coefficients for codimension 2 bifurcations of limit cycles are not computed by any available software. For discrete systems, such coefficients can be computed and they can even be used to start the computation of codimension 1 cycles rooted in such points; see [12, 14]. We will exploit this possibility.

In this paper we investigate a map in the plane for a pair of populations, first studied in [15, 16]. Danca et al. [15] investigated Neimark-Sacker bifurcations numerically. Murakami [16] discussed its branch points, flip bifurcations, and Neimark-Sacker bifurcations, establishing the sub- or supercritical character of the flip and Neimark-Sacker bifurcations by an explicit reduction to the center manifolds, obtaining a prediction for the invariant curve that branches off at the NS point. We undertake an analysis of the dynamics of the iterates of the map. This paper is organized as follows. In Section 2, we first discuss the map and the stability and bifurcations of its fixed points, proving the results in [16] by direct computations of the normal form coefficients. Next, in Section 3, we numerically compute curves of fixed points and bifurcation curves of the map and its iterates up to order 16 under variation of one and two parameters. We compute the critical normal form coefficients of all computed codim-1 and codim-2 bifurcations. These coefficients are powerful tools to compute stability boundaries of the map and its iterates and to switch to other bifurcation curves. In Section 4, we study more details on the bifurcation scenario of the system around a Neimark-Sacker bifurcation point. We conclude our work in Section 5 with a discussion of the obtained results.

2. The Model, the Fixed Points, Their Stability, and Bifurcations

In this paper, we study the map

$$F : \begin{pmatrix} x \\ y \end{pmatrix} \longmapsto \begin{pmatrix} ax(1-x) - bxy \\ dxy \end{pmatrix}, \tag{2.1}$$

which is analogous to (1.1) for the case of predators and prey with nonoverlapping generations; see [16, 17]. It can also be seen as an approximate discretization of the continuous-time Lotka-Volterra model

$$\begin{aligned} \dot{x}(t) &= \alpha_0 x(t)(1 - x(t)) - \alpha m x(t) y(t), \\ \dot{y}(t) &= m x(t) y(t) - \beta y(t), \end{aligned} \tag{2.2}$$

which is a simplification of (1.1) in which the intraspecific competition of the predator is ignored and the carrying capacity of the prey is 1. x and y represent the densities of the prey and predator, and α_0, α, m, and β are nonnegative parameters. Applying the forward Euler scheme to system (2.2) with the stepsize $1/\beta$ and assuming $\alpha_0/\beta \gg 1$, we obtain the map (2.1) with nonnegative parameters $a = \alpha_0/\beta$, b = $\alpha m/\beta$, and $d = m/\beta$.

We note that in (2.1) one of the two parameters b, d can be removed by a rescaling of y. So, the system is in reality a two-parameter system and fully equivalent to the system studied in [16]. We will generally choose d, a as the unfolding parameters in the bifurcation study. In a way, it is the simplest possible discrete predator-prey model and, therefore, allows a reasonably complete analytical treatment as far as the fixed points of the map are concerned. However, we will see that even in this case the behaviour of cycles is very complicated and can only be studied by numerical methods.

We naturally start the bifurcation analysis of (2.1) with the calculation of the fixed points. These are the solutions (x^*, y^*) to

$$a x^*(1 - x^*) - b x^* y^* = x^*, \quad d x^* y^* = y^*. \tag{2.3}$$

The origin $E_1 = (0, 0)$ is a fixed point of (2.1) but is of little interest. Two further nontrivial fixed points are $E_2 = ((a - 1)/a, 0)$ and $E_3 = (1/d, 1/b(a(1 - (1/d)) - 1))$. We note that E_2 is biologically possible only if its coordinates are nonnegative, that is, $a \geq 1$. E_3 is biologically possible only if the following conditions hold:

(i) $a > 1$,

(ii) $d \geq a/(a - 1)$.

We start the local bifurcation analysis of the map (2.1) by linearization of F around each of its fixed points. The Jacobian matrix $J(x, y)$ is given by

$$J(x, y) = \begin{pmatrix} a - 2ax - by & -bx \\ dy & dx \end{pmatrix}. \tag{2.4}$$

The characteristic equation of $J(x, y)$ is given by

$$\lambda^2 - \mathrm{tr}(J) + \det(J) = 0, \tag{2.5}$$

where $\mathrm{tr}(J) = a - 2ax - by + dx$ and $\det(J) = dxa - 2dx^2 a$.

2.1. Stability and Bifurcation of E_1

Proposition 2.1. *The fixed point E_1 is asymptotically stable for $0 \leq a < 1$. It loses stability via branching for $a = 1$ and there bifurcates to E_2.*

Proof. Eigenvalues of the Jacobian at E_1 are a and 0. So, E_1 is stable if $a < 1$ and loses stability at $a = 1$. In (a, x)-space E_1 forms the curve $(a, 0)$ with tangent vector $(1, 0)$. E_2 is represented in (a, x)-space by the curve $(a, (a-1)/a)$. When $a = 1$, these curves intersect at $(1, 0)$ and the tangent vector in (a, x)-space is $(1, 1)$, so it is clear that E_1 branches to E_2 for $a = 1$. □

2.2. Stability and Bifurcation of E_2

The Jacobian matrix of (2.1) at E_2 is given by

$$J(E_2) = \begin{pmatrix} -a+2 & \dfrac{-b(a-1)}{a} \\ 0 & \dfrac{d(a-1)}{a} \end{pmatrix}. \tag{2.6}$$

Proposition 2.2. *The fixed point E_2 is linearly asymptotically stable if and only if $a \in]1, 3[$ and $d < a/(a-1)$. Moreover, it loses stability:*

(i) *via branching for $a = 1$ and there bifurcates to E_1,*

(ii) *via branching for $d = a/(a-1)$ and there bifurcates to E_3 if $1 < a < 3$,*

(iii) *via a supercritical flip for $a = 3$ if $d < 3/2$.*

Proof. The multipliers of $J(E_2)$ are $\lambda_1 = -a + 2$ and $\lambda_2 = d(a-1)/a$. The fixed point E_2 is asymptotically stable if and only if $|\lambda_1| < 1$ and $|\lambda_2| < 1$, that is, if and only if $a \in]1, 3[$ and $d < a/(a-1)$. Boundary points of the stability region must satisfy one of three conditions: $a = 1$, $d = a/(a-1)$, or $a = 3$.

In the first case, the conditions $d < a/(a-1)$ and $a < 3$ are satisfied for nearby values $a > 1$, hence this is a real stability boundary. In Proposition 2.1, we proved that this is a branch point and the new branch consists of E_1 points.

In the second case, this is a stability boundary only if $1 < a < 3$. The Jacobian (2.6) then has an eigenvalue +1 and it is checked easily that these boundary points are also E_3 points.

In the third case, this is a stability boundary only if $d < 3/2$. In this case, $\lambda_1 = -1$ which means that E_2 loses stability via a period doubling point. For supercriticality of the period doubling point, it is sufficient to show that the corresponding critical normal form coefficient b_1,

$$b_1 = \frac{1}{6}\left\langle p, C(q,q,q) + 3B\Big(q, (I-A)^{-1}B(q,q)\Big)\right\rangle, \tag{2.7}$$

derived by center manifold reduction is positive; see [9], Ch. 8 and [14]. Here, $A = J(E_2)$, and $B(\cdot,\cdot)$,$C(\cdot,\cdot,\cdot)$ are the second- and third- order multilinear forms, respectively, and p and

q are the left and right eigenvectors of A for the eigenvalue -1, respectively. These vectors are normalized by $\langle p, q\rangle = 1$, $\langle q, q\rangle = 1$, where $\langle \cdot\cdot \rangle$ is the standard scalar product in $\mathbb{R}^2$. We obtain

$$q = \begin{pmatrix} q_1 \\ q_2 \end{pmatrix} = \begin{pmatrix} 1 \\ 0 \end{pmatrix},$$
$$p = \begin{pmatrix} p_1 \\ p_2 \end{pmatrix} = \begin{pmatrix} 1 \\ \dfrac{2b}{3+2d} \end{pmatrix}. \tag{2.8}$$

The components of the multilinear form $B(q, q)$ are given by

$$\left[B(q,q)\right]_1 = \sum_{j,k=1}^{2} \frac{\partial^2 (ax(1-x) - bxy)}{\partial x_j \partial x_k} q_j q_k = -2aq_1q_1 = -6,$$
$$\left[B(q,q)\right]_2 = \sum_{j,k=1}^{2} \frac{\partial^2 (dxy)}{\partial x_j \partial x_k} q_j q_k = 2dq_1q_2 = 0, \tag{2.9}$$

where the state variable vector is for ease of notation generically denoted by $(x_1, x_2)^T$ instead of $(x, y)^T$.

Let $\zeta = (I - A)^{-1} B(q, q)$, then we have $\zeta = \binom{-3}{0}$ and find

$$\left[B(q,\zeta)\right]_1 = -2aq_1\zeta_1 = -2a(-3) = 18, \qquad \left[B(q,\zeta)\right]_2 = dq_1\zeta_2 = 0. \tag{2.10}$$

The third-order multilinear form $C(q, q, q)$ is identically zero. The critical normal form coefficient b_1 is given by

$$b_1 = \frac{1}{6} p^T \begin{pmatrix} 54 \\ 0 \end{pmatrix} = 9, \tag{2.11}$$

which is clearly positive. This completes the proof of supercriticality of the flip point at E_2. □

The stability region $\Omega^S_{E_2}$ of E_2, as obtained in Proposition 2.2, is shown in Figure 1.

2.3. *Stability and Bifurcation of* E_3

To study the stability of E_3, we use the Jury's criteria; see [6, Section A2.1]. Let $F(\lambda) = \lambda^2 - \mathrm{tr}(J(E_3))\lambda + \det(J(E_3))$ be the characteristic polynomial of $J(E_3)$.

According to the Jury's criteria, E_3 is asymptotically stable if the following conditions hold:

$$\begin{aligned} F(-1) &= 1 + \operatorname{tr}(J(E_3)) + \det(J(E_3)) > 0, \\ F(1) &= 1 - \operatorname{tr}(J(E_3)) + \det(J(E_3)) > 0, \\ &1 - \det(J(E_3)) > 0. \end{aligned} \tag{2.12}$$

At E_3, we have:

$$J(E_3) = \begin{pmatrix} \dfrac{d-a}{d} & -\dfrac{b}{d} \\ \dfrac{da-a-d}{b} & 1 \end{pmatrix}. \tag{2.13}$$

We note that $\operatorname{tr}(J(E_3)) = (2d-a)/d$ and $\det(J(E_3)) = a(d-2)/d$ are independent of b.

Proposition 2.3. *E_3 is linearly asymptotically stable if and only if one of the following mutually exclusive conditions holds:*

(i) $3/2 < d < 9/4$ *and* $d/(d-1) < a < 3d/(3-d)$,

(ii) $d = 9/4$ *and* $1.8 = d/(d-1) < a < d/(d-2) = 3d/(3-d) = 9$,

(iii) $d > 9/4$ *and* $d/(d-1) < a < d/(d-2)$.

Proof. The criterion $F(1) > 0$ is easily seen to be equivalent to the condition

$$a > \frac{d}{d-1}, \quad d > 1, \tag{2.14}$$

or equivalently,

$$d > \frac{a}{a-1}, \quad a > 1. \tag{2.15}$$

Next, the criterion $\det(J(F3)) < 1$ is easily seen to be equivalent to

$$a < \frac{d}{d-2} \quad \text{if } d > 2. \tag{2.16}$$

The criterion $F(-1) > 0$ translates as

$$a < \frac{3d}{3-d} \quad \text{if } d < 3. \tag{2.17}$$

□

In Figure 1, the parts of the 3 curves $a = d/(d-1)$, $a = d/(d-2)$, and $a = 3d/(3-d)$ where a and d are positive are depicted (resp., for $d > 1$, $d > 2$, and $0 < d < 3$). The curves

$a = d/(d-1)$ and $a = 3d/(3-d)$ intersect solely at $(d = 3/2, a = 3)$ and the curves $a = d/(d-2)$ and $a = 3d/(3-d)$ at $(d = 9/4, a = 9)$. It follows from the figure that the 3 inequalities are fullfilled when (i), (ii), or (iii) holds. This can also easily be shown algebraic. In Figure 1, the stability region Ω^S_{E3} of E_3 is thus the union of Ω^{S1}_{E3} and Ω^{S2}_{E3} (which correspond to (i) and (iii) in this proposition, resp.), and the open interval that separates them (and corresponds to (ii)).

Proposition 2.4. *E_3 loses stability:*

(i) *via a flip point when $3/2 < d < 9/4$ and $a = 3d/(3-d)$,*

(ii) *via a Neimark-Sacker point when $9/4 < d$ and $a = d/(d-2)$,*

(iii) *via a branch point when $d > 3/2$ and $a = d/(d-1)$ where it bifurcates to E_2,*

(iv) *via a branch-flip (BPPD) point when $d = 3/2$ and $a = 3$,*

(v) *via a resonance 1 : 2 point when $d = 9/4$ and $a = 9$.*

Proof. By Proposition 2.3 the stability boundary of E_3 consists of parts of three curves, namely,

(1) Curve 1: $a = 3d/(3-d)$.

(2) Curve 2: $a = d/(d-2)$.

(3) Curve 3: $a = d/(d-1)$.

The points of Curve 1 which are on the stability boundary of E_3 satisfy $F(-1) = 0$, that is, they have an eigenvalue -1 and, thus, are period doubling points. The points of Curve 2 which are on the stability boundary satisfy $\det(J(E_3)) = 1$, that is, they have two eigenvalues with product 1 and, thus, are Neimark-Sacker points. The points of Curve 3 which are on the stability boundary satisfy $F(1) = 0$, that is, they have an eigenvalue 1. It can be checked easily that E_3 then branches to E_2.

Combining this with Proposition 2.2 we find that the interior points of the boundary parts of Curves 1, 2, and 3 form the sets described in parts (i), (ii), and (iii) of Proposition 2.3, respectively.

At the intersection of Curves 1 and 3 (when $d = 3/2$ and $a = 3$), the point is a branch-flip point (BPPD) with eigenvalues -1 and 1. The intersection point of Curves 1 and 2 (when $d = 9/4$ and $a = 9$) is a resonance 1 : 2 point with double eigenvalue -1. □

Proposition 2.5. *The flip point in Proposition 2.4, part (i), is subcritical.*

Proof. For the subcriticality of the flip bifurcation, it is sufficient to show that the normal form coefficient b_1 in (2.7) is always negative. By using the same procedure as we used in the proof of Proposition 2.2, we obtain

$$q = \begin{pmatrix} q_1 \\ q_2 \end{pmatrix} = \begin{pmatrix} 1 \\ \dfrac{d(2d-3)}{b(d-3)} \end{pmatrix}, \qquad p = \begin{pmatrix} p_1 \\ p_2 \end{pmatrix} = \begin{pmatrix} 1 \\ \dfrac{b}{2d} \end{pmatrix}. \tag{2.18}$$

To simplify computations, we do not normalize p and q, since rescaling does not change the sign of b_1 provided that $\langle p, q\rangle$ is positive (it can be proved easily that this is the case). $B(q,q)$ is computed as

$$B(q,q) = \begin{pmatrix} -4d \\ \dfrac{2d^2(2d-3)}{b(d-3)} \end{pmatrix}. \tag{2.19}$$

Let $\zeta = (I-A)^{-1}B(q,q)$, then we have $\zeta = \begin{pmatrix} d \\ -d^2(4+(3/(3-d)))/b \end{pmatrix}$ and find

$$B(q,\zeta) = \begin{pmatrix} \dfrac{2d^2}{3-d}(6-d) - 2ad \\ \dfrac{-2d^3(6-d)}{b(3-d)} \end{pmatrix}. \tag{2.20}$$

The third-order multilinear form $C(q,q,q)$ is zero. The critical normal form coefficient $b_1 = (-1/2)d^3/(3-d)$, which is clearly negative for $3/2 < d < 9/4$. This completes the proof of subcriticality of the flip point. □

Proposition 2.6. *The Neimark-Sacker point in Proposition 2.4, part (ii), is supercritical.*

Proof. To prove the supercriticality of the Neimark-Sacker point, it is sufficient to show that the real part of the corresponding critical normal form coefficient d_1,

$$\begin{aligned} d_1 &= \frac{1}{2}e^{-i\theta_0}\langle p, C(q,q,\overline{q}) + 2B(q,h_{1100}) + B(\overline{q},h_{2000})\rangle, \\ h_{1100} &= (I_n - A)^{-1}B(q,\overline{q}), \\ h_{2000} &= \left(e^{2i\theta_0}I_n - A\right)^{-1}B(q,q), \end{aligned} \tag{2.21}$$

is negative; see [14]. Here, $\theta_0 (0 < \theta_0 < \pi)$ is the argument of the critical multiplier, $A = J(E_3)$, and $B(\cdot,\cdot)$, $C(\cdot,\cdot,\cdot)$ are the second- and third-order multilinear forms, respectively. p and q are the left and right eigenvectors of A

$$\begin{aligned} Aq &= e^{i\theta_0}q, \\ A^T p &= e^{-i\theta_0}p. \end{aligned} \tag{2.22}$$

These vectors are normalized by $\langle p,q\rangle = 1, \langle q,q\rangle = 1$, where $\langle p,q\rangle = p^H q$ is the Hermitian inner product in $\mathbb{C}^2$. In the Neimark-Sacker point, $a = d/(d-2)$ ($d > 9/4$, so $d-2 > 0$). We get

$$A = \begin{pmatrix} \dfrac{d-3}{d-2} & -\dfrac{b}{d} \\ \dfrac{d}{b(d-2)} & 1 \end{pmatrix}, \tag{2.23}$$

with characteristic polynomial $\lambda^2-((2d-5)/(d-2))\lambda+1$. It follows that $\Re(\lambda) = (d-(5/2))/(d-2)$ and $\Im(\lambda) = \sqrt{d-(9/4)}/(d-2)$, so $e^{i\theta_0} = 1/(d-2)(d-(5/2)+i\sqrt{d-(9/4)})$. The eigenvectors are

$$q = \begin{pmatrix} (d-2)\dfrac{b}{d} \\ -\dfrac{1}{2} - i\sqrt{d-\dfrac{9}{4}} \end{pmatrix},$$
$$p = \frac{d\left(2d-(9/2)-i\sqrt{d-(9/4)}\right)}{b(4d^2-17d+18)} \begin{pmatrix} 1 \\ \dfrac{b}{d}\left(\dfrac{1}{2} - i\sqrt{d-\dfrac{9}{4}}\right) \end{pmatrix}, \tag{2.24}$$

where q is not normalized since rescaling of q does not change the sign of d_1 (this can be proved easily) and we can simplify the computations by not normalizing. The calculation of the components of $B(q,\overline{q})$ gives us

$$B(q,\overline{q}) = -b(d-2)\begin{pmatrix} \dfrac{b}{d} \\ 1 \end{pmatrix}, \tag{2.25}$$

and it follows that

$$h_{1100} = b(d-2)\begin{pmatrix} \dfrac{b(d-2)}{d} \\ -2 \end{pmatrix}. \tag{2.26}$$

The remaining calculations are done with the help of Maple. The calculation of h_{2000} gives us

$$h_{2000} = \frac{-2(d-2)^3 b}{-50d^2+135d+6i\sqrt{4d-9}d^2-29i\sqrt{4d-9}d-119+35i\sqrt{4d-9}+6d^3}$$
$$\cdot \begin{pmatrix} \dfrac{b}{d}\left(17d-7i\sqrt{4d-9}d-23+11i\sqrt{4d-9}-3d^2+i\sqrt{4d-9}d^2\right) \\ i\sqrt{4d-9}d+22-2i\sqrt{4d-9}+4d^2-19d \end{pmatrix}, \tag{2.27}$$

where

$$e^{2i\theta_0} = \frac{1}{(d-2)^2}\left(d^2-6d+\frac{17}{2}+i(2d-5)\sqrt{d-\frac{9}{4}}\right). \tag{2.28}$$

For $B(\overline{q}, h_{2000})$ and $B(q, h_{1100})$, we obtain

$$B(\overline{q}, h_{2000}) = \frac{2(d-2)^3 b^2}{-50d^2 + 135d + 6i\sqrt{4d-9}d^2 - 29i\sqrt{4d-9}d - 119 + 35i\sqrt{4d-9} + 6d^3} \cdot \begin{pmatrix} \frac{b}{d}\left(32d - 6i\sqrt{4d-9}d - 29 + 9i\sqrt{4d-9} - 13d^2 + i\sqrt{4d-9}d^2 + 2d^3\right) \\ i\sqrt{4d-9}d^2 + 2d - 8i\sqrt{4d-9}d - 2d^3 + 7d^2 - 17 + 13i\sqrt{4d-9} \end{pmatrix},$$
$$B(q, h_{1100}) = \frac{(d-2)^2 b^2}{2} \begin{pmatrix} b\left(1 + i\sqrt{4d-9}\right) \\ -5 - i\sqrt{4d-9} \end{pmatrix}. \tag{2.29}$$

The third-order multilinear form $C(q, q, q)$ is identically zero, so we get

$$\begin{aligned} d_1 &= \frac{1}{2} e^{-i\theta_0} p^H \left(2B(q, h_{1100}) + B(\overline{q}, h_{2000})\right) \\ &= \frac{1}{4}\left(-2d + 5 + i\sqrt{4d-9}\right)\left(4d - 9 + i\sqrt{4d-9}\right) b^2 d \\ &\quad \times \left(31d^2 + i\sqrt{4d-9}d^3 + 44 - 5d^3 - 64d - 12i\sqrt{4d-9} - 7i\sqrt{4d-9}d^2 + 16i\sqrt{4d-9}d\right) \\ &\quad \times (4d-9)^{-1}\left(-50d^2 + 135d + 6i\sqrt{4d-9}d^2 - 29i\sqrt{4d-9}d - 119 + 35i\sqrt{4d-9} + 6d^3\right)^{-1}. \end{aligned} \tag{2.30}$$

The real part of d_1 equals $-1/2b^2 d$ (exact up to a positive factor due to the nonnormalization of q), which is clearly negative. This completes the proof of supercriticality of the Neimark-Sacker point in Proposition 2.4, part (ii). □

The stability regions (i) and (iii) of E_3 obtained in Proposition 2.3 are depicted as Ω_{E3}^{S1} and Ω_{E3}^{S2}, respectively, in Figure 1. The region (ii) is the open interval on the common boundary of Ω_{E3}^{S1} and Ω_{E3}^{S2}. We have a complete description of the stability region of E_3 for all parameter combinations.

The biological interpretation of Figure 1 is as follows. The situation with no prey and no predators exists for all parameter values but is stable only in Ω_{E1}^{S}, that is, for $a < 1$. The situation with a fixed number of prey but no predators exists for all $a > 1$ but is stable only in Ω_{E2}^{S}. Coexistence of fixed nonzero numbers of prey and predators is possible whenever $a > 1$ and $d > a/(a-1)$ but is stable only in the union of Ω_{E3}^{S1} and Ω_{E3}^{S2}.

3. Numerical Bifurcation Analysis of E_2 and E_3

In this section, we perform a numerical bifurcation analysis by using the MATLAB package Cl_MatContM; see [12, 14]. The bifurcation analysis is based on continuation methods, whereby we trace solution manifolds of fixed points while some of the parameters of the map vary; see [18]. We note that in a two-parameter setting the boundaries of stability domains of cycles are usually curves of codimension 1 bifurcations, which necessarily have to be computed by numerical continuation methods.

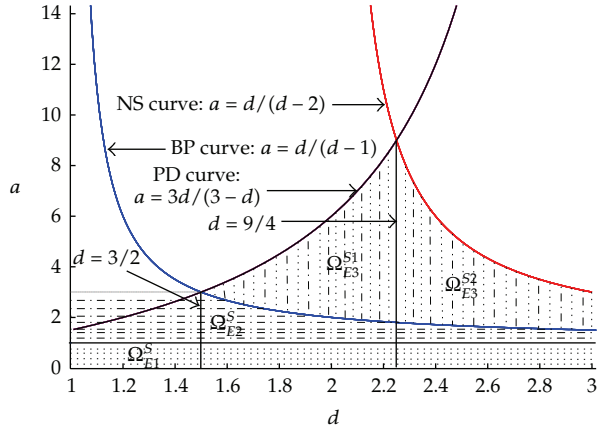

Figure 1: Stability regions in (d, a)-space. Ω^S_{E1}, Ω^S_{E2} are the stability regions of E_1 and E_2, respectively. The stability region Ω^S_{E3} of E_3 is the union of Ω^{S1}_{E3} and Ω^{S2}_{E3} (which correspond to (i) and (iii) in Proposition 2.3, resp.), and the open interval that separates them (and corresponds to (ii) in Proposition 2.3).

To validate the model, we compute a number of stable cycles for parameter values in the regions where we claim they exist; these stable cycles were found by orbit convergence, independently of the continuation methods. They are represented in the Figures 2, 6, 11, and 14. Similarly, a stable closed invariant curve was computed by orbit convergence and is represented in Figure 4. The computation of an Arnold tongue in Section 3.5 by a continuation method also validates our computations.

3.1. *Numerical Bifurcation of* E_2

By continuation of $E_2 = (0.5; 0)$ starting from $a = 2$, $b = 0.2$, $d = 1.4$, in the stable region of E_2 with a free, we see that E_2 is stable when $1 < a < 3$. It loses stability via a supercritical period doubling point (PD, the corresponding normal form coefficient is $9 > 0$) when $a = 3$, and via a branch point (BP) when a crosses 1.4. The output of *Run 1* is given by:

```
label = BP, x = (0.000000 0.000000 1.000000)
label = PD, x = (0.666667 0.000000 3.000000)
normal form coefficient of PD = 9.000000e+000
```

The first two entries of `x` are the coordinate values of the fixed point E_2, and the last entry of `x` is the value of the free parameter a at the corresponding bifurcation point. We note that the normal form coefficient of the PD point is 9, confirming (2.11). We note furthermore that the detected bifurcation points in this run are in accordance with the statement of Proposition 2.2.

Beyond the PD point the dynamics of (2.1) is a stable 2-cycle. Cl_MatContM allows to switch to the continuation of this 2-cycle. It loses stability at a supercritical PD point:

```
label = PD, x = (0.849938 0.000000 3.449490)
normal form coefficient of PD = 4.062566e+002
```

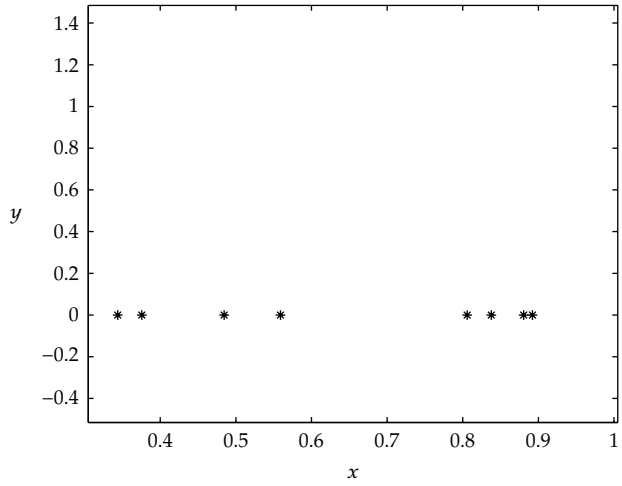

Figure 2: A stable 8-cycle of (2.2) for $a = 3.571920967580968$, $b = 0.2$, $d = 1.4$.

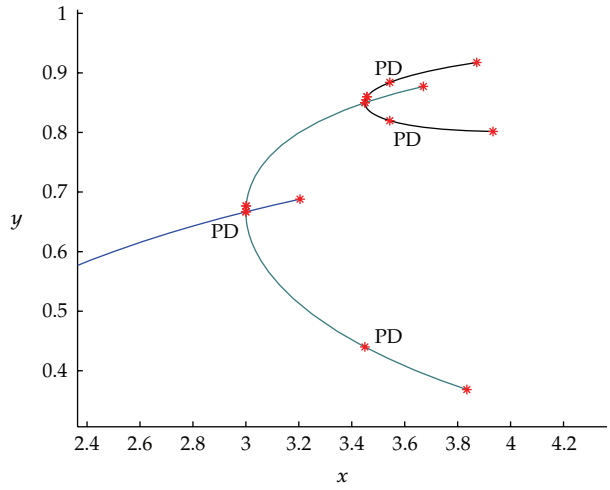

Figure 3: Curves of fixed points of the first, second and fourth iterates.

A stable 4-cycle is born when $a > 3.449490$. It loses stability at a supercritical PD point:

```
label = PD, x = (0.884050 0.000000 3.544090)

normal form coefficient of PD = 1.617268e+004
```

Thus, when $a > 3.544090$ a stable 8-cycle emerges. A stable 8-cycle is given by $C_8 = \{X_1^8, \ldots, X_8^8\}$, where $X_1^8 = (0.880450408535962, 0)$ where $a = 3.571920967580968$, $b = 0.2$, and $d = 1.4$. This 8-cycle is represented in Figure 2. In this situation there are no predators and the number of prey repeats itself every 8 time spans. Switchings at PD points of the second and fourth iterates are given in Figure 3.

We note that for E_2 the map (2.1) is a logistic map. In fact, in this case the predator becomes extinct and the prey undergoes the period-doubling bifurcation to chaos when further increasing the parameter a; see [19].

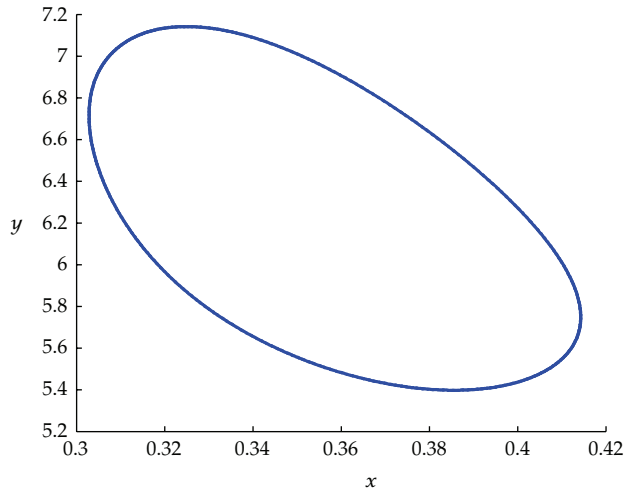

Figure 4: A stable closed invariant curve for $a = 3.5$, $b = 0.2$, and $d = 2.83$.

Continuation of E_2 starting from the same parameter values as in *Run 1*, with d as free parameter, leads to:

```
label = BP, x = (0.500000 0.000000 2.000000)
```

The appearance of a branch point is consistent with Proposition 2.2 part (ii) which states that E_2 bifurcates to E_3 when $b = d = a/(a-1) = 2$.

3.2. *Numerical Bifurcation of* E_3

We now consider $E_3 = (0.454545; 4.545454)$ which is in the stable region for the parameter values $a = 3.5$, $b = 0.2$, and $d = 2.2$ (stability follows from Proposition 2.3 part (i)). We do a numerical continuation of E_3 with control parameter d, and call this *Run 2*. The output of *Run 2* is given by:

```
label = PD, x = (0.619048 1.666667 1.615385)
normal form coefficient of PD = −5.905026e−001
label = NS, x = (0.357143 6.250000 2.800000)
normal form coefficient of NS = −6.971545e−002
```

E_3 is stable when $1.615385 < d < 2.8$. It loses stability via a supercritical Neimark-Sacker (NS) point when $d = 2.8$, which is consistent with Proposition 2.4 part (ii) $(d/(d-2) = 3.5 = a)$. It also loses stability through a subcritical PD point when $d = 1.615385$, which is consistent with Propositions 2.5 and 2.4 part (i) since $3d/(3-d) = 3.5 = a$.

The dynamics of the system prior to the PD point consists of an unstable 2-cycle that coexists with a stable fixed point. Beyond the NS point the dynamics of the system consists of a stable closed invariant which coexists with unstable fixed points of (2.1). For $d = 2.83$, a stable closed invariant curve is created around the unstable fixed point E_3 (see Figure 4).

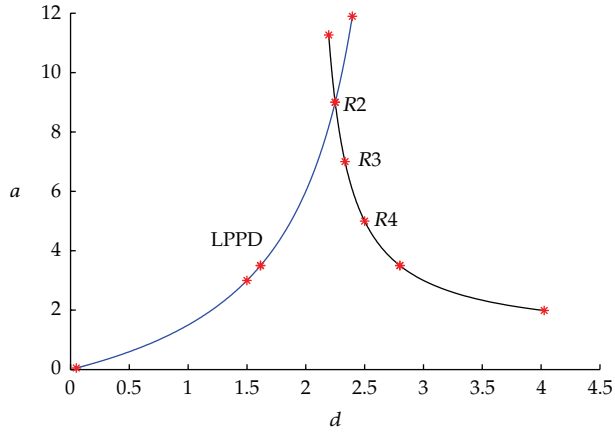

Figure 5: Flip and Neimark-Sacker bifurcation curves starting from points in *Run 2*. We note that the LPPD point is in reality a BPPD point.

Now, we compute the period doubling curve, with a and d free, by starting from the PD point detected in *Run 2*. We call this *Run 3*.

```
label = LPPD, x = (0.666667 0.00000 3 1.500000)
Normal form coefficient for LPPD:[a/e, be] = −3.333334e−001,
4.541342e−006
label = R2, x = (0.444444 20.000000 9.000000 2.250000)
Normal form coefficient for R2:[c, d] = 1.197634e−001, −7.185806e−001
```

Two codim-2 bifurcation points are detected on the flip curve, namely, a fold-flip LPPD and a resonance 2 bifurcation *R2*. We note that the LPPD point is in reality a branch-flip (BPPD) point, which by the software is detected as an LPPD point since BPPD points are ungeneric on a curve of PD points. This curve is shown in Figure 5 (left curve). Now, we compute the NS curve, with a and d free parameters, by starting from the NS point of *Run 2*. We call this *Run 4*.

```
label = R4, x = (0.400000 10.000000 5.000000 2.500000 −0.000000)
Normal form coefficient of R4: A = −1.240347e+000 + 6.201737e−001 i
label = R3, x = (0.428571 15.000000 7.000000 2.333333 −0.500000)
Normal form coefficient of R3: Re(c_1) = −5.000000e−001
label = R2, x = (0.444444 20.000000 9.000000 2.250000 −1.000000)
Normal form coefficient of R2: [c, d] = 1.197646e−001, −7.185574e−001
```

The computed curve of NS points is also shown in Figure 5 (right curve). The codim-2 bifurcations that are computed along the Neimark-Sacker curve are a resonance 1 : 2 (*R2*), resonance 1 : 3 (*R3*), and a resonance 1 : 4 (*R4*) point. In addition to the coordinates of the bifurcation point, parameter values and the real part of the Neimark-Sacker multiplier at the bifurcation point are output. We note that the PD curve crosses over the NS curve $a = d/(d-2)$ at a resonance 1 : 2 (*R2*) point, which is consistent with Proposition 2.4 part (v). It also hits the BP curve $a = d/(d-1)$ at a branch-flip point BPPD which is consistent with Proposition 2.4 part (iv).

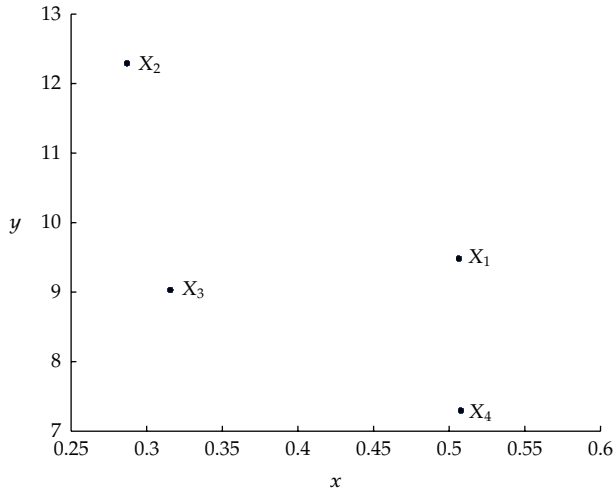

Figure 6: A stable 4-cycle near an *R4* point for $a = 4.99$, $b = 0.2$, and $d = 2.56$.

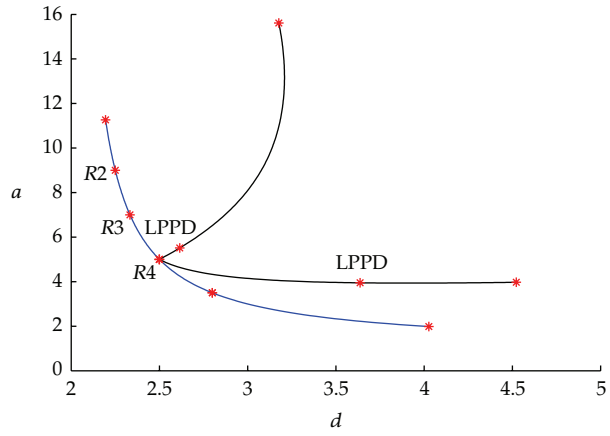

Figure 7: Twofold curves (LP^4) emanate from an *R4* point on an NS curve.

3.3. Orbits of Period 4, 8, 16 and 32

The normal form coefficient A of the *R4* point in *Run 4* satisfies $|A| > 1$, hence two cycles of period 4 of the map are born. A stable 4-cycle for $a = 4.99$, $b = 0.2$, and $d = 2.56$ is given by: $C_4 = \{X_1, X_2, X_3, X_4\}$, where $X_1 = (0.506291269909196, 9.483616960226117)$. We present this cycle in Figure 6. In order to compute the stability region of this 4-cycle, we compute the twofold curves of the fourth iterate rooted at the *R4* point. These curves exist since $|A| > 1$, see [9], and switching from an *R4* point to the fold curves of the fourth iterate is supported by Cl_MatContM. The stable fixed points of the fourth iterate exist in the wedge between the

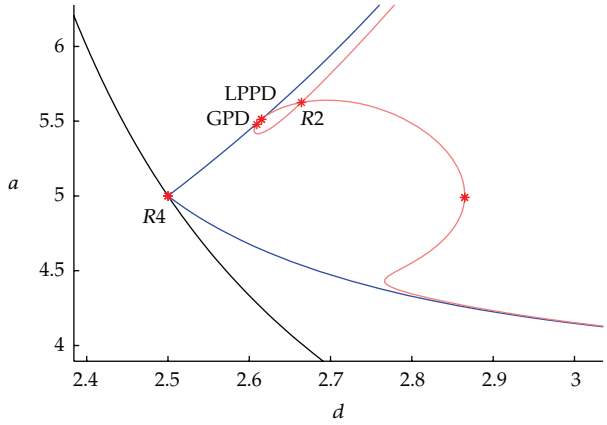

Figure 8: Twofold curves (LP^4) of the fourth iterate emanate from an *R4* point, and a flip curve of the fourth iterate (PD^4) is rooted at an LPPD point.

twofold curves. The output of this continuation, *Run 5*, is given below. The curves are shown in Figure 7.

```
label = LPPD, x = (0.077546 7.084151 3.948550 3.637018)
Normal form coefficient for LPPD:[a/e, be] = −1.638977e−001,
−1.231773e+001
label = LPPD, x = (0.540029 8.419070 5.511767 2.615029)
Normal form coefficient for LPPD:[a/e, be] = 7.735689e−001,
−8.261238e−002
```

We can further compute the stability boundaries of the 4-cycle. This region is bounded by the two just computed limit point curves and a period doubling curve of the fourth iterate rooted at the detected LPPD points on the branches of LP^4 curves. Continuation of the flip curve of the fourth iterate emanated at the LPPD of *Run 5* is given below. We call this *Run 6*.

```
label = LPPD, x = (0.862908 2.257241 3.948550 3.637018)
Normal form coefficient for LPPD:[a/e, be] = −1.638977e−001,
−9.218471e+001
label = LPPD, x = (0.540029 8.419070 5.511767 2.615029)
Normal form coefficient for LPPD:[a/e, be] = 7.735689e−001,
−8.261238e−002
label = GPD, x = (0.541277 8.238085 5.478361 2.609243)
Normal form coefficient of GPD = 6.483721e−001
label = R2, x = (0.582936 7.330070 5.625162 2.664169)
Normal form coefficient for R2:[c, d]= 6.130829e−002, −3.509615e+000
```

By superposing the flip curve on Figure 7, we obtain Figure 8. We further compute a curve of fixed points of the fourth iterate starting from the 4-cycle C_4 presented in Figure 6,

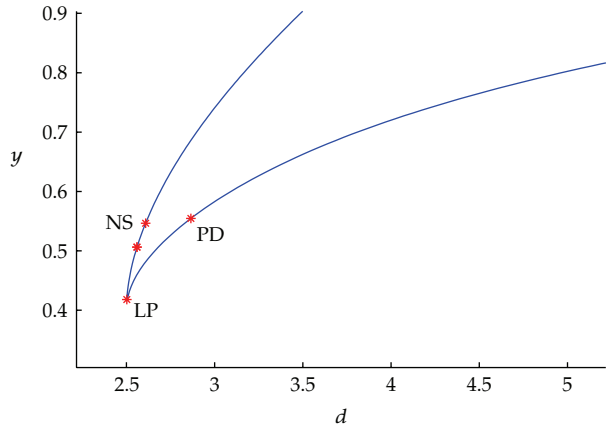

Figure 9: Curve of fixed points of the fourth iterate starting from the 4-cycle C_4.

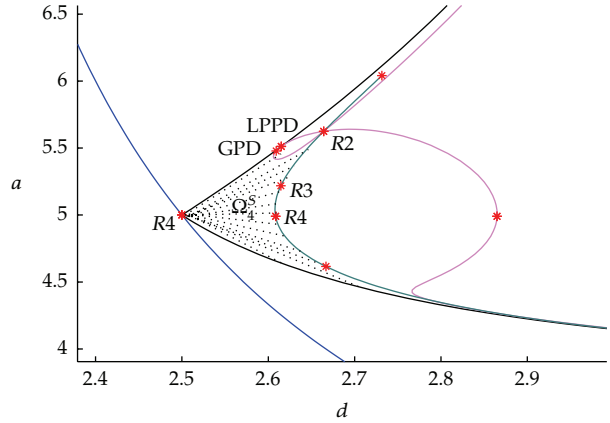

Figure 10: Stability region Ω_S^4 of the 4-cycle C_4. The boundaries consist of NS, LP^4, PD^4, and NS^4 curves.

with control parameter d. The output of this continuation, *Run 7*, is given below. The curve is presented in Figure 9.

```
label = LP, x = (0.418135 9.911757 2.502419)
normal form coefficient of LP = −2.095861e−001
label = PD, x = (0.554614 8.335785 2.864961)
normal form coefficient of PD = 1.909178e−001
label = NS, x = (0.546431 9.030507 2.608544)
normal form coefficient of NS = −2.177981e+000
```

The 4-cycle remains stable when $2.502419 < d < 2.608544$. Now, we compute an NS-curve starting from the computed NS point in *Run 8* and call this *Run 9*. This curve is superposed on Figure 8 and is depicted in Figure 10.

```
label = R4, x = (0.594620 7.423051 4.615965 2.666797 0.000000)
Normal form coefficient of R4: A = −4.453277e+000 + −1.491255e+000 i
```

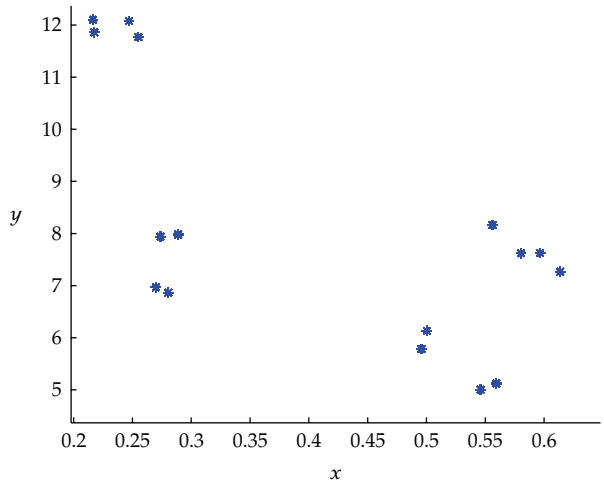

Figure 11: A stable 16-cycle around the *R4* point of *Run 9* for $a = 4.68$, $b = 0.2$, and $d = 2.66$.

```
label = R3, x = (0.529139 9.928228 5.218594 2.614545 −0.500000)

Normal form coefficient of R3: Re(c_1) = −6.065820e+000

label = R2, x = (0.513005 11.383897 5.625162 2.664169 −1.000000)

Normal form coefficient of R2: [c, d] = 1.004097e−001, −5.657220e+000
```

The stability region Ω_S^4 of the 4-cycle C_4 is bounded by the LP^4, PD^4, and NS^4 curves (see Figure 10).

Now, we consider the *R4* point computed in *Run 9*. Since the corresponding normal form coefficient A satisfies $|A| > 1$, two cycles of period 16 of the map are born. A stable 16-cycle for $a = 4.68$, $b = 0.2$, and $d = 2.66$ is given by $C_{16} = \{X_1, X_2, \ldots, X_{16}\}$, where $X_1 = (0.596607820551550, 7.625016168527653)$. We present this cycle in Figure 11.

In order to compute the stability region of this 16-cycle, we compute twofold curves of the sixteenth iterate rooted at the *R4* point. These curves exist since $|A| > 1$. The stable fixed points of the sixteenth iterate exist in the wedge between the twofold curves. The output of this continuation, *Run 10*, is given below, and the fold curves are shown in Figure 12.

```
label = LPPD, x = (0.557836 8.068783 4.651131 2.670940)

Normal form coefficient for LPPD:[a/e, be] = 1.235611e+001,
3.799853e−001

First Lyapunov coefficient for second iterate = 3.799853e−001

label = LPPD, x = (0.519225 8.927562 4.765661 2.658381)

Normal form coefficient for LPPD:[a/e, be] = 9.129886e+000,
5.166118e+000

First Lyapunov coefficient for second iterate = 5.166118e+000

label = LPPD, x = (0.469475 10.678780 5.153847 2.636682)

Normal form coefficient for LPPD:[a/e, be] = 1.298255e−001,
−4.388341e+000
```

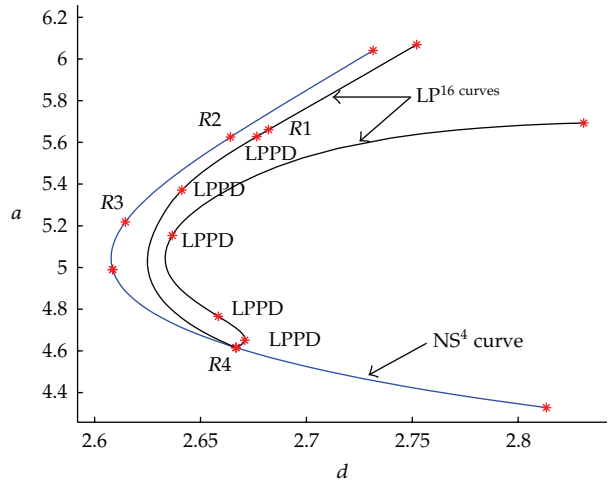

Figure 12: Twofold curves (LP^{16}) emanate from an *R4* point on the NS^4 curve.

```
label = LPPD, x = (0.580415 9.268192 5.370935 2.641181)

Normal form coefficient for LPPD:[a/e, be] = 1.528369e+000,
6.631508e+001

First Lyapunov coefficient for second iterate = 6.631508e+001

label = LPPD, x = (0.578148 9.853334 5.628124 2.676611)

Normal form coefficient for LPPD:[a/e, be] = −9.656910e−001,
−2.522009e+004

label = R1, x = (0.577592 9.941486 5.660840 2.682153)

normal form coefficient of R1 = −1
```

We further compute a curve of fixed points of the sixteenth iterate starting from the 16-cycle C_{16} presented in Figure 11, with control parameter a. The output of this continuation, *Run 11*, is given below. The curve is presented in Figure 13.

```
label = LP, x = (0.598114 7.473352 4.646130)

normal form coefficient of LP = 2.965904e+000

label = PD, x = (0.595604 7.701225 4.700640)

normal form coefficient of PD = 2.829176e+002
```

The 16-cycle remains stable when $4.646130 < d < 4.700640$. The dynamics of the system beyond the supercritical PD is a stable 32-cycle which coexists with the unstable fixed points of the sixteenth iterate of the system.

A stable 32-cycle for $a = 4.7071$, $b = 0.2$, and $d = 2.66$ is given by: $C_{32} = \{X_1, X_2, \ldots, X_{32}\}$, where $X_1 = (0.619778764655944, 7.243979650146042)$. We present this cycle in Figure 14.

Now, we compute a PD-curve starting from the computed PD point in *Run 10*, and call this *Run 12*. This curve is superposed on Figure 12, and is depicted in Figure 15. The boundaries of the stability region Ω_S^{16} of the 16-cycle consist of the LP^{16} and PD^{16} curves, as illustrated in Figure 15.

```
label = LPPD, x = (0.600292 7.504485 4.651131 2.670940)
```

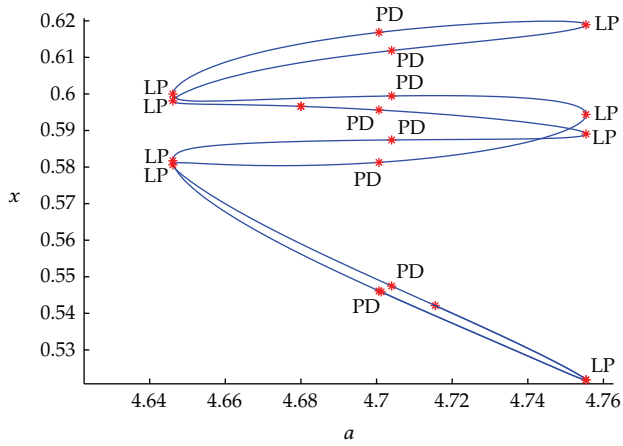

Figure 13: Curve of fixed points of the sixteenth iterate starting from the 16-cycle C_{16}.

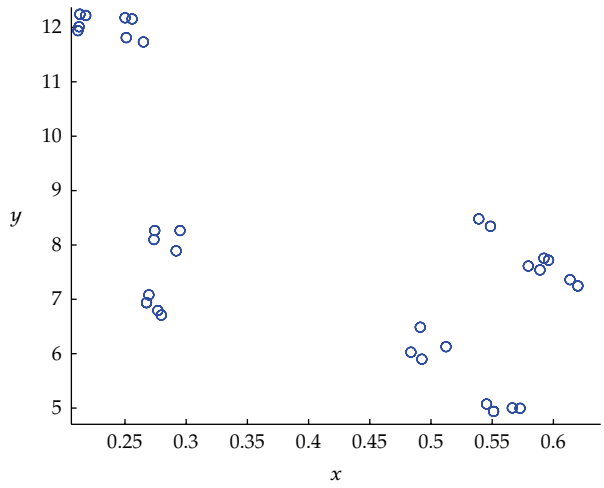

Figure 14: A stable 32-cycle for $a = 4.7071$, $b = 0.2$, and $d = 2.66$.

```
Normal form coefficient for LPPD:[a/e, be] = 1.235612e+001,
1.579190e+003

First Lyapunov coefficient for second iterate = 1.579190e+003

label = LPPD, x = (0.587235 7.998201 4.765661 2.658381)

Normal form coefficient for LPPD:[a/e, be] = 9.129867e+000,
9.328278e+002

First Lyapunov coefficient for second iterate = 9.328278e+002

label = GPD, x = (0.529363 9.922888 5.130266 2.635413)

Normal form coefficient of GPD = 1.292549e+007

label = LPPD, x = (0.526233 10.046755 5.153847 2.636682)
```

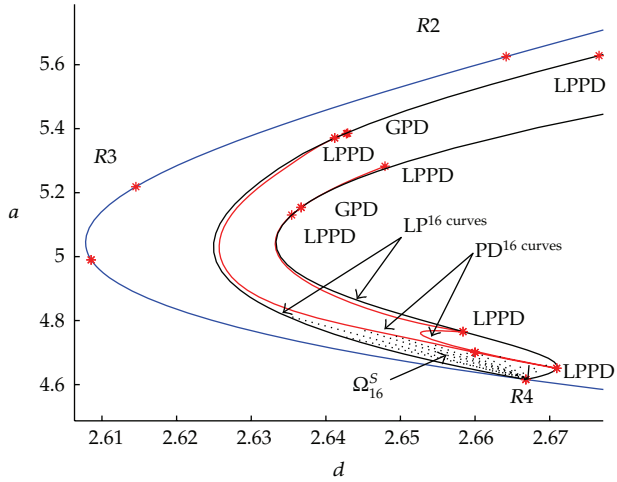

Figure 15: Stability region Ω_S^{16} of the 16-cycle C_{16}. The boundaries consist of LP^{16} and PD^{16} curves.

```
Normal form coefficient for LPPD:[a/e, be] = 1.298254e−001,
−7.143714e+002

label = LPPD, x = (0.521191 10.840009 5.370935 2.641181)

Normal form coefficient for LPPD:[a/e, be] = 1.528369e+000,
1.217953e+002

First Lyapunov coefficient for second iterate = 1.217953e+002

label = GPD, x = (0.521992 10.863772 5.384512 2.642770)

Normal form coefficient of GPD = −6.188850e+003
```

3.4. Orbits of Period 3

Next, we consider the resonance 1 : 3 (*R3*) point in *Run 4*. Since its normal form coefficient is negative, the bifurcation picture near the *R3* point is qualitatively the same as presented in [9, Figure 9.12]. In particular, there is a region near the *R3* point where a stable invariant closed curve coexists with an unstable fixed point. For parameter values close to the *R3* point, the map has a saddle cycle of period three.

Furthermore, a Neutral Saddle bifurcation curve of fixed points of the third iterate emanates [9, Chapter 9]. We compute this curve by branch switching at the *R3* point. This curve is presented in Figure 16.

3.5. Computation of Arnold Tongues

It is well known that near a Neimark-Sacker curve there exists a dense array of resonance tongues, generalizing the isolated tongue of period 4 in Figure 7. The tongues locally form an open and dense set of the parameter plane. There are also quasiperiodic invariant circles in between that correspond to a set of positive measure in the parameter plane.

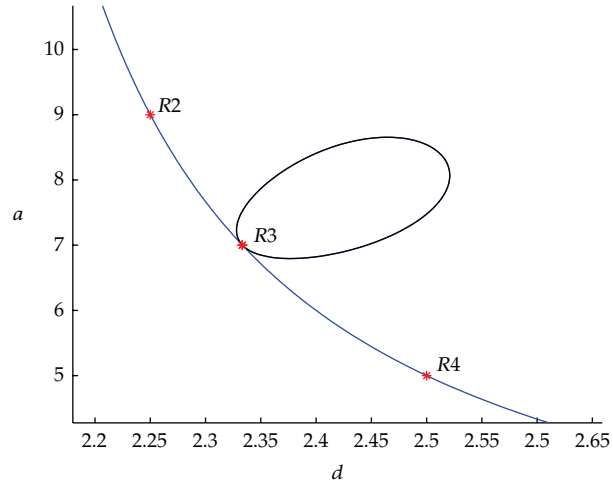

Figure 16: Curve of Neutral Saddle bifurcations of the third iterate for $b = 0.2$.

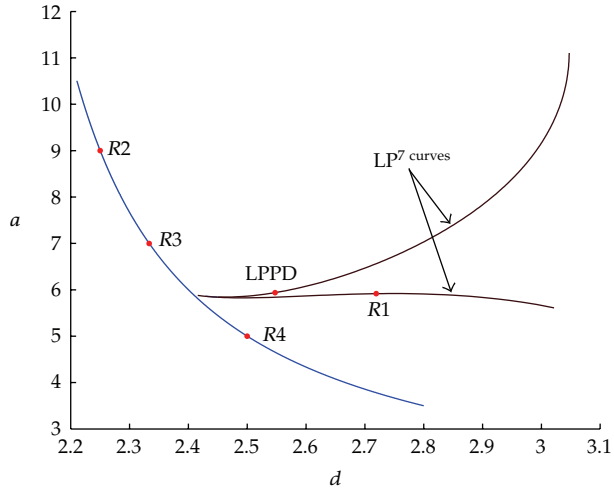

Figure 17: An Arnold tongue rooted in a weak $2:7$ resonant Neimark-Sacker point.

So far, no numerical methods have been implemented to specifically compute the boundaries of the resonance tongues that are rooted in weakly resonant Neimark-Sacker points (unlike the strong resonant $1:4$ case). However, since they are limit point curves of fixed points of cycles with known periods, they can be computed relatively easily if the cycles inside the tongue are globally stable (which depends on the criticality of the Neimark-Sacker curve and the noncritical multipliers as well). It is sufficient to find a fixed point of cycles inside the tongue by orbit convergence and to continue it in one free parameter to find a point on the boundary of the Arnold tongue as a limit point of cycles. From this, the boundary curves can be computed by a continuation in two free parameters.

In Figure 17, we present an Arnold Tongue rooted in a weak $2:7$ resonant Neimark-Sacker point. Its computation started from a stable 7-cycle with $x = 0.401985064603439$,

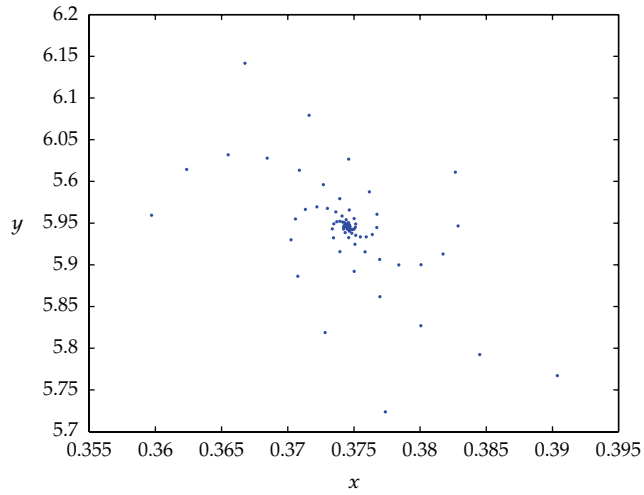

Figure 18: An attracting fixed point for system (2.2) for $a = 3.5$, $b = 0.2$, and $d = 2.67$.

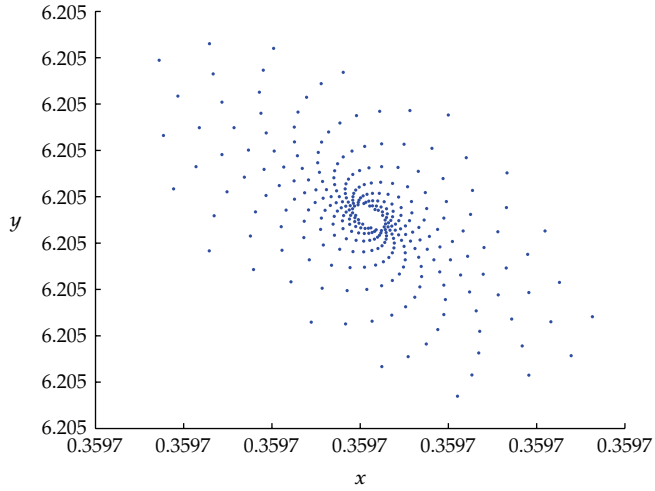

Figure 19: Phase portrait for the system (2.2) before the NS point ($a = 3.5$, $b = 0.2$, and $d = 2.78$).

$y = 12.930999111981340$, $a = 5.844728289174310$, $b = 0.2$, and $d = 2.45$. We note that the boundary curves contain further bifurcation points.

4. Numerical Simulation

To reveal the qualitative dynamical behaviours of (2.2) near the NS point in *Run 1*, we present a complete bifurcation sequence that is observed for different values of d. We fix the parameters $a = 3.5$, $b = 0.2$ and assume that d is free.

Figure 18 shows that E_3 is a stable attractor for $d = 2.67$. We note that for the given parameters value, E_3 is a stable fixed point consistent with Proposition 2.3 part (iii). The behaviour of (2.2) at $d = 2.78$, so before the NS point at $d = 2.8$, is depicted in Figure 19.

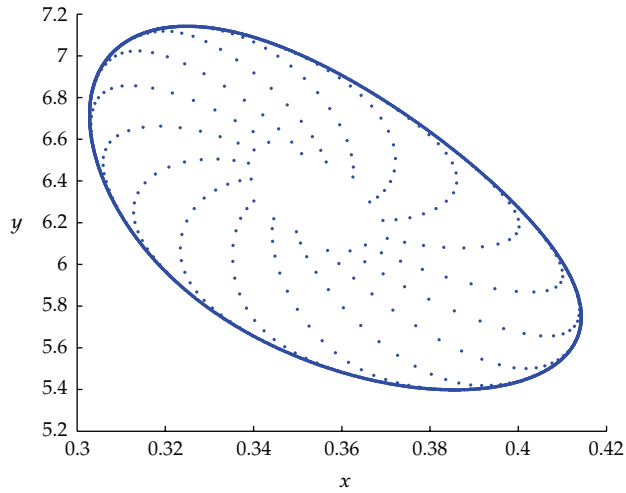

Figure 20: Phase portrait for the system (2.2) for $a = 3.5$, $b = 0.2$, and $d = 2.81$.

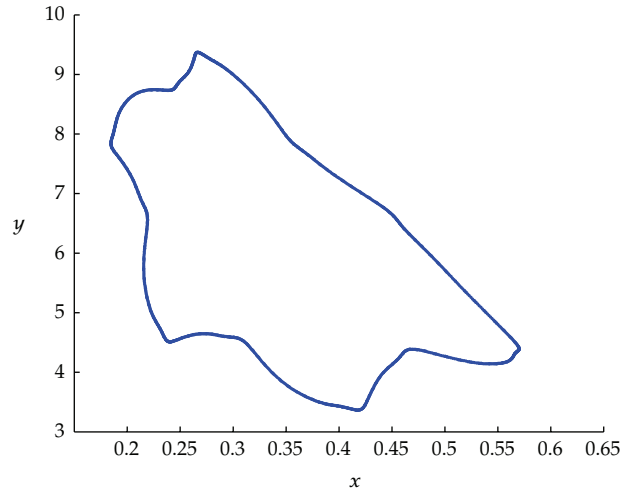

Figure 21: The breakdown of the closed invariant curve of the system (2.2) for $a = 3.5$, $b = 0.2$, and $d = 3.13$.

Figure 20 demonstrates the behaviour of the model after the NS bifurcation, for $d = 2.81$. From Figures 19 and 20 it turns out that the fixed point E_3 loses its stability through an NS bifurcation, when d varies from 2.78 to 2.81. The dynamics of (2.2) beyond the NS point is a stable closed invariant curve which coexists with unstable fixed point E_3.

As d is increased further, however, the phase portrait starts to fold. We see that the circle, after being stretched, shrunk, and folded, creates new phenomena due to the breakdown of the closed curve; see Figure 21 for $d = 3.13$.

For increasing d, we obtain the multiple invariant closed curves brought about the NS bifurcation point of iterates of (2.2). In these cases, higher bifurcations of the torus occurs as the system moves out of quasiperiodic region by increasing d. The dynamics move from one closed curve to another periodically, but the dynamics in each closed curve, may be periodic or quasiperiodic. Figure 22 presents the set of closed curves around the NS bifurcation.

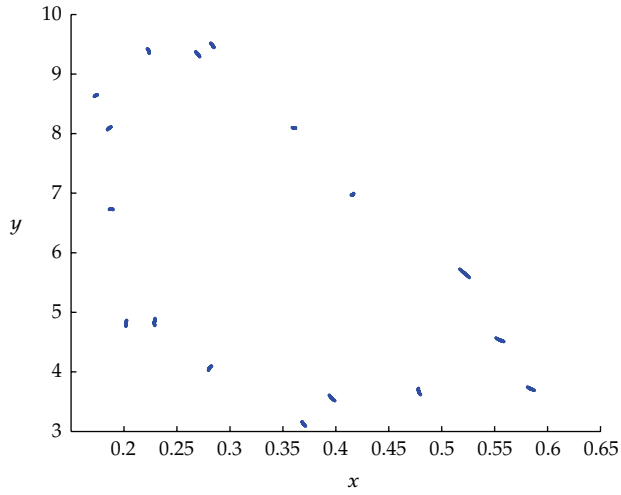

Figure 22: The existence of multiple closed curves of the system (2.2) for $a = 3.5$, $b = 0.2$, and $d = 3.215$.

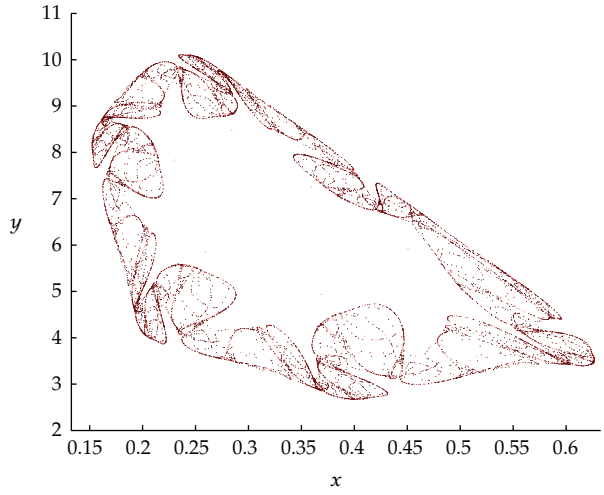

Figure 23: Chaotic attractor for the system (2.2) for $a = 3.5$, $b = 0.2$, and $d = 3.25$.

Moreover, the closed curves may break and lead to multiple fractal tori on which the dynamics of (2.2) are chaotic. Figures 23 and 24 present strange attractors for (2.2) with $d = 3.25$ and $d = 3.8$, respectively, which exhibit a fractal structure.

5. Concluding Remarks

In this paper, we studied a planar map that models a predator-prey interaction with nonoverlapping generations. We derived analytically a complete description of the stability regions of the fixed points of the system, namely, E_1, E_2, and E_3. We showed that the system undergoes branching, period doubling, and Neimark-Sacker bifurcations. In particular, we determined criticality of the flip, and Neimark-Sacker bifurcations for E_2 and E_3 analytically

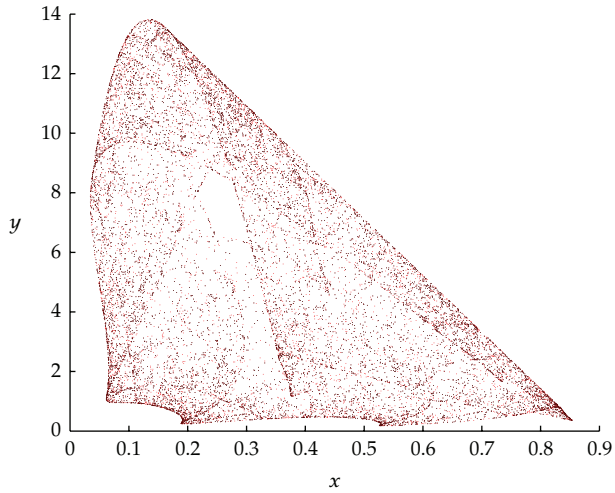

Figure 24: Chaotic attractor for the system (2.2) for $a = 3.5$, $b = 0.2$, and $d = 3.8$.

by direct computation of the normal form coefficients without explicit reduction to the center manifold. To support the analytical results and reveal the further complex behaviour of the system, we employed numerical continuation methods to compute curves of codimension 1 and 2 bifurcation points. In particular, we computed curves of fixed points of different cycles as well as curves of fold, flip and Neimark-Sacker bifurcations of the fourth iterate, and fold and flip bifurcations of the sixteenth iterate. These curves form stability boundaries of different cycles of the system. These tasks were possible by means of the computation of normal form coefficients and branch-switching algorithms. We further used numerical simulation methods to reveal chaotic behaviours and a strange attractor near the Neimark-Sacker bifurcation.

Acknowledgments

This paper was greatly improved by the comments of four reviewers who read the paper from different viewpoints. The authors thank them all and thank the editorial staff of DDNS for the fast and efficient handling of the manuscript. R. K. Ghaziani also would like to thank Shahrekord University for the financial support through a research grant.

References

[1] A. A. Berryman, "The origins and evolution of predator-prey theory," *Ecology*, vol. 73, no. 5, pp. 1530–1535, 1992.

[2] M. Fan and K. Wang, "Periodic solutions of a discrete time nonautonomous ratio-dependent predator-prey system," *Mathematical and Computer Modelling*, vol. 35, no. 9-10, pp. 951–961, 2002.

[3] H. Fang and J. D. Cao, "Global existence for positive periodic solutions to a class of predator-prey systems," *Journal of Biomathematics*, vol. 15, no. 4, pp. 403–407, 2000.

[4] H. I. Freedman, *Deterministic Mathematical Models in Population Ecology*, vol. 57 of *Monographs and Textbooks in Pure and Applied Mathematics*, Marcel Dekker, New York, NY, USA, 1980.

[5] B. S. Goh, *Management and Analysis of Biological Populations*, Elsevier, Amsterdam, The Netherlands, 1980.

[6] J. D. Murray, *Mathematical Biology*, vol. 19 of *Biomathematics*, Springer, Berlin, Germany, 2nd edition, 1993.
[7] A. D. Bazykin, *Nonlinear Dynamics of Interacting Populations*, vol. 11 of *World Scientific Series on Nonlinear Science. Series A: Monographs and Treatises, A. I. Khibnik and B. Krauskopf, Eds.*, World Scientific, River Edge, NJ, USA, 1998.
[8] V. I. Arnold, *Geometrical Methods in the Theory of Ordinary Differential Equations*, vol. 250 of *Grundlehren der Mathematischen Wissenschaften*, Springer, New York, NY, USA, 1983.
[9] Y. A. Kuznetsov, *Elements of Applied Bifurcation Theory*, vol. 112 of *Applied Mathematical Sciences*, Springer, New York, NY, USA, 3rd edition, 2004.
[10] H. W. Broer, K. Saleh, V. Naudot, and R. Roussarie, "Dynamics of a predator-prey model with non-monotonic response function," *Discrete and Continuous Dynamical Systems. Series A*, vol. 18, no. 2-3, pp. 221–251, 2007.
[11] E. J. Doedel, R. A. Champneys, T. F. Fairgrieve, Yu. A. Kuznetsov, B. Sandstede, and X. J. Wang, "AUTO2000: Continuation and Bifurcation Sotware for Ordinary Differential Equations (with HomCont), Users' Guide," Concordia University, Montreal, Canada 1997–2000, http://indy.cs.concordia.ca.
[12] W. Govaerts and Yu. A. Kuznetsov, "Matcont: a Matlab software project for the numerical continuation and bifurcation study of continuous and discrete parameterized dynamical systems," http://sourceforge.net/.
[13] R. P. Agarwal, *Difference Equations and Inequalities: Theory, Methods, and Applicationa*, vol. 228 of *Monographs and Textbooks in Pure and Applied Mathematics*, Marcel Dekker, New York, NY, USA, 2nd edition, 2000.
[14] W. Govaerts, R. K. Ghaziani, Yu. A. Kuznetsov, and H. G. E. Meijer, "Numerical methods for two-parameter local bifurcation analysis of maps," *SIAM Journal on Scientific Computing*, vol. 29, no. 6, pp. 2644–2667, 2007.
[15] M. Danca, S. Codreanu, and B. Bakó, "Detailed analysis of a nonlinear prey-predator model," *Journal of Biological Physics*, vol. 23, no. 1, pp. 11–20, 1997.
[16] K. Murakami, "Stability and bifurcation in a discrete-time predator-prey model," *Journal of Difference Equations and Applications*, vol. 13, no. 10, pp. 911–925, 2007.
[17] S. Li and W. Zhang, "Bifurcations of a discrete prey-predator model with Holling type II functional response," *Discrete and Continuous Dynamical Systems. Series B*, vol. 14, no. 1, pp. 159–176, 2010.
[18] E. L. Allgower and K. Georg, *Numerical Continuation Methods: An Introduction*, vol. 13 of *Springer Series in Computational Mathematics*, Springer, Berlin, Germany, 1990.
[19] R. L. Kraft, "Chaos, Cantor sets, and hyperbolicity for the logistic maps," *The American Mathematical Monthly*, vol. 106, no. 5, pp. 400–408, 1999.